Impact of silicon doping on the structure and crystallization of a vanadium-tellurite glass

Yan, Jiajia; Zhao, T.Y.; Shi, N.; Zhan, H.B.; Ren, J.J.; Zhang, Y.F.; Yue, Yuanzheng

Published in:
Journal of Non-Crystalline Solids

DOI (link to publication from Publisher):
10.1016/j.jnoncrysol.2022.121651

Publication date:
2022

Document Version
Publisher's PDF, also known as Version of record

Citation for published version (APA):
Yan, J., Zhao, T. Y., Shi, N., Zhan, H. B., Ren, J. J., Zhang, Y. F., & Yue, Y. (2022). Impact of silicon doping on the structure and crystallization of a vanadium-tellurite glass. *Journal of Non-Crystalline Solids*, *589*, Article 121651. https://doi.org/10.1016/j.jnoncrysol.2022.121651

Journal of Non-Crystalline Solids 589 (2022) 121651

Contents lists available at ScienceDirect

Journal of Non-Crystalline Solids

journal homepage: www.elsevier.com/locate/jnoncrysol

Impact of silicon doping on the structure and crystallization of a vanadium-tellurite glass

Jiajia Yan [a], Tongyao Zhao [b], Nian Shi [b], Hongbing Zhan [c], Jinjun Ren [b], Yanfei Zhang [d,*], Yuanzheng Yue [a,*]

[a] *Department of Chemistry and Bioscience, Aalborg University, Fredrik Bajers Vej 7H, Aalborg DK-9220, Denmark*
[b] *Key Laboratory of Materials for High Power Laser, Shanghai Institute of Optics and Fine Mechanics, Chinese Academy of Sciences, Shanghai 201800, China*
[c] *College of Materials Science and Engineering, Fuzhou University, Fuzhou 350108, China*
[d] *School of Materials Science and Engineering, Qilu University of Technology (Shandong Academy of Sciences), Jinan 250353, China*

ARTICLE INFO

Keywords:
V_2O_5-TeO_2 glass
Nano-silicon
Heat treatment
Silicon-glass interaction
Structural change
Crystallization

ABSTRACT

We studied the effect of silicon doping on the structure and crystallization behavior of $50V_2O_5$-$50TeO_2$ (mol%) (VT) glass by performing solid-state nuclear magnetic resonance (NMR), Fourier-transform infrared spectroscopy (FTIR), X-ray diffraction (XRD), and differential scanning calorimetry (DSC). We observed two interesting phenomena. First, when the mixture of glass and Si is heated in argon to 560 K ($1.1T_g$), Si starts to react with VT glass and is oxidized to amorphous silica, being confirmed by NMR and FTIR. Second, Si suppresses the formation of the $Te_2V_2O_9$ phase in VT glass during heating process up to 650 K (about $1.3T_g$), whereas it leads to the formation of the new crystalline phase $TeVO_4$ during heating to 725 K ($1.4T_g$). We discuss the origin of these two phenomena by considering the changes both in glass structure and in the redox reaction.

1. Introduction

It is known that silicon (Si) has high initial theoretical capacity (>4000 mA h/g) as anode material in Li-ion batteries (LIBs), but in reality, has not been applied since it undergoes a severe volume change during lithiation/delithiation, leading to a drastic decay of the capacity [1]. It is also known that vanadium-tellurite (VT) glasses are a promising anode material with higher cycling stability for LIBs, although it has lower capacity than Si [2,3]. The reason for the high cycling stability of VT glasses lies in their unique structure feature (e.g., not purely 3D tetrahedral network) that exhibits higher liquid fragility, semi-conducting and stronger crystallization tendency upon heating compared to most of the conventional oxide glasses with tetrahedral network. During discharging/charging process, electrons can cause formation of polarons, and thus, high electronic conductivity can be realized by polaron-hopping in $V^{4+}{-}O{-}V^{5+}$ chains ($V^{4+}{-}O{-}V^{5+}\rightarrow V^{5+}{-}O{-}V^{4+}$) [2,4]. The cycling ability of VT glass anode has been attributed to formation of the electrochemically active γ-Li_3VO_4 nanocrystals induced by insertion/extraction of Li ions. The nanocrystals lead to toughening of glass matrix and thereby increase the cycling stability. Thus, it is anticipated that the incorporation of nano Si into VT glass could lead to the synergetic effect, i.e., to both enhanced capacity and increased cycling stability of the anode for LIBs.

Here, the key question is whether the VT glass can buffer the volume change of Si during lithiation/delithiation and thereby suppress the decay of the anode performance if the two types of materials are properly combined. To answer this question, we need to investigate how they can be bonded together physically or chemically during heating process, and to find out how the Si-doping affects the crystallization behavior of VT glasses. To the best of our knowledge, such studies have not been reported in literature.

To conduct the above-mentioned investigations, we prepared the mixture of 10 wt% Si and 90 wt% VT glass using the physical mixing and subsequently sintering method. As is known, the heterogeneous nucleation in glass is easier to occur than the homogenous nucleation as the former has a lower nucleation energy barrier [5]. When nano-silicon powder is introduced into glass, the chemical heterogeneity and interfaces are created, and hence, the crystallization tendency is expected to be enhanced. The question is whether this common knowledge also applies to the impact of Si doping on the crystallization of VT glass. To

---

* Corresponding author.
* Corresponding author.
E-mail addresses: zhang-yanfei@hotmail.com (Y. Zhang), yy@bio.aau.dk (Y. Yue).

https://doi.org/10.1016/j.jnoncrysol.2022.121651
Received 19 February 2022; Received in revised form 14 April 2022; Accepted 15 April 2022

Table 1
The detailed heat-treatment procedures of $50V_2O_5$-$50TeO_2$ glass powder (VT) and $50V_2O_5$-$50TeO_2$ glass doped with Si powder (VTS).

Sample Name	Heat-Treatment Procedures 1st DSC upscan	 2nd DSC upscan	 3rd DSC upscan
VT-650 or VTS-650	To 650 K	/	/
VT-650-2 or VTS-650-2	To 650 K	To 650 K	/
VT-650-3 or VTS-650-3	To 650 K	To 650 K	To 650 K
VT-650-725 or VTS-650-725	To 650 K	To 725 K	/
VT-650-725-2 or VTS-650-725-2	To 650 K	To 725 K	To 725 K

do so, the mixed powder samples were heat-treated to different temperatures in argon (see Experimental section). The crystallization behavior is characterized by using the differential scanning calorimetry (DSC) and X-ray diffraction (XRD). The nature of bonding between Si nano powder and VT glass, as well as the structure changes of VT glass and Si upon crystallization were analyzed by performing the nuclear magnetic resonance (NMR) and Fourier-transform infrared spectroscopy (FTIR). We discussed the mechanism of the crystallization in the Si doped VT glass.

2. Experimental

The $50V_2O_5$-$50TeO_2$ (in mol %) glass prepared via the melt-quenching method [2] is chosen as the basic glass to composite with nano-Si. The $50V_2O_5$-$50TeO_2$ glass powder (VT) with a narrow size distribution between 5 and 10 μm was obtained by crushing and sieving the bulk sample. 100 mg commercial nano-silicon powder (about 20-60 nm particle size) was added into 0.9 g glass powder and then mixed thoroughly, which is referred to as VTS.

We conducted dynamic heat-treatment on both VT and VTS samples by the differential scanning calorimeter (DSC) (Jupiter 449C, Netzsch). Specifically, the VT and VTS were firstly subjected to a DSC upscan to 775 K at 10 K/min, respectively, to detect their thermal events, e.g., the glass transition temperature (T_g) and the crystallization onset temperature (T_c) (see Fig. S1). Based on this result, the new VT and VTS samples are upscanned to 545 K (a temperature just over the glass transition peak) and then downscanned at 10 K/min in argon to eliminate the glass thermal history. After that, different DSC scanning procedures were performed at the same heating and cooling rates of 10 K/min. VTS samples were upscanning to T_g (509 K), $1.1T_g$ (560 K), $1.2T_g$ (610 K), $1.3T_g$ (≈650 K), $1.4T_g$ (≈725 K), $1.6T_g$ (815 K), $1.8T_g$ (916 K), $2T_g$ (1018 K), and $2.1T_g$ (1067 K), in order to study the temperature at which Si starts to react with VT glass. VT and VTS samples after upscanning to 650 K (a temperature between T_{c2} and T_{c3}, which is denoted in Fig. S1), referred to as VT-650 and VTS-650, respectively, underwent the second and third DSC upscanning to investigate their crystallization behaviors. In detail, some VT-650 and VTS-650 samples were heat-treated to 650 K for the second and third upscans, others were upscanned to 725 K (a temperature between T_{c3} and the melting peak, which is denoted in Fig. S1) for the second and third times, which are referred to as VT-650-2,VTS-650-2, VT-650-3, VTS-650-3, VT-650-725, VTS-650-725, VT-650-725-2, and VTS-650-725-2, respectively, according to the upscanning temperatures and times. The detailed heat-treatment procedure is given in Table 1.

The crystal phases in VT and VTS after various heat treatment were identified on a PANalytical X-ray diffractometer with Cu Kα (λ = 1.5406 Å) radiation. NMR measurement for VT, VTS were performed on a Bruker Avance III HD 500 M spectrometer (11.7 T). We detected ^{51}V and ^{125}Te spectra for VT and VTS, and ^{29}Si spectra for VTS. The ^{29}Si, ^{51}V and ^{125}Te NMR measurements were conducted at the resonance frequencies of 99.4, 131.7 and 159.1 MHz, respectively. ^{29}Si MAS NMR spectra were measured at a spinning rate of 6.0 kHz. Relaxation delays of 200 s were used, and chemical shift is referenced to Tetrakis (tetramethyl) silicate silane (= -9.7 ppm). ^{51}V Hahn echo NMR experiments were operated at a spinning rate of 0 kHz with the pulse length of 2.4 μs. ^{125}Te static wideband uniform-rate smooth truncation QCPMG (WURST-QCPMG) NMR spectra were obtained using the WURST-80 pulse sequence and an 8-step phase cycle, employing 50-μs excitation and refocusing pulses (liquid nutation frequency 8.1 kHz). FTIR spectra of Si and VTS were obtained by a Bruker Invenio S infrared spectrometer in the wavenumber range of 400 to 1400 cm^{-1} at room temperature with a resolution of 4 cm^{-1}.

3. Results

To investigate how and at which temperature Si and VT glass were

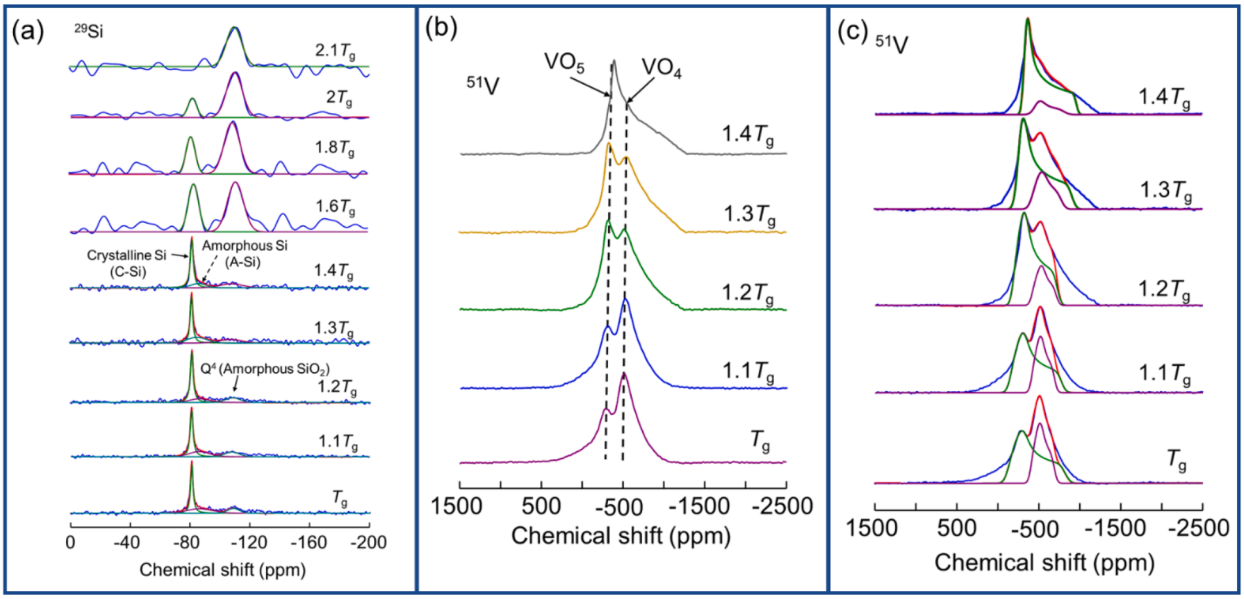

Fig. 1. ^{29}Si and ^{51}V NMR spectra of VTS upscanned in DSC to different temperatures at 10 K/min in argon. (a) ^{29}Si NMR spectra of VTS upscanned to $T_g \sim 2.1T_g$, (b) ^{51}V NMR spectra of VTS upscanned to $T_g \sim 1.4T_g$, (c) deconvolution of ^{51}V NMR spectra shown in (b). Purple and green curves represent the VO_4 and VO_5 contributions, respectively.

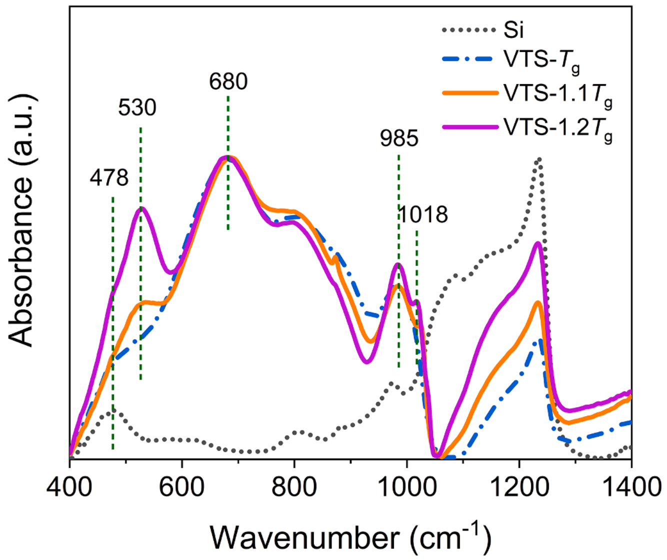

Fig. 2. FTIR spectra of Si and VTS after upscanning in DSC to T_g, 1.1T_g and 1.2T_g at 10 K/min in argon.

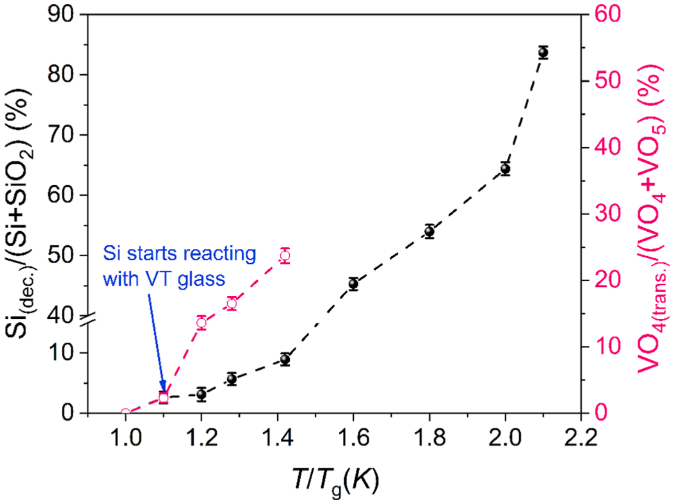

Fig. 3. The dependences of both $Si_{(dec.)}/(Si+SiO_2)$ and $VO_{4(trans.)}/((VO_4+VO_5)$ on the maximum DSC upscanning temperatures for VTS samples. The T/T_g represents the ratio of the DSC upscanning temperature to the glass transition temperature of VTS.

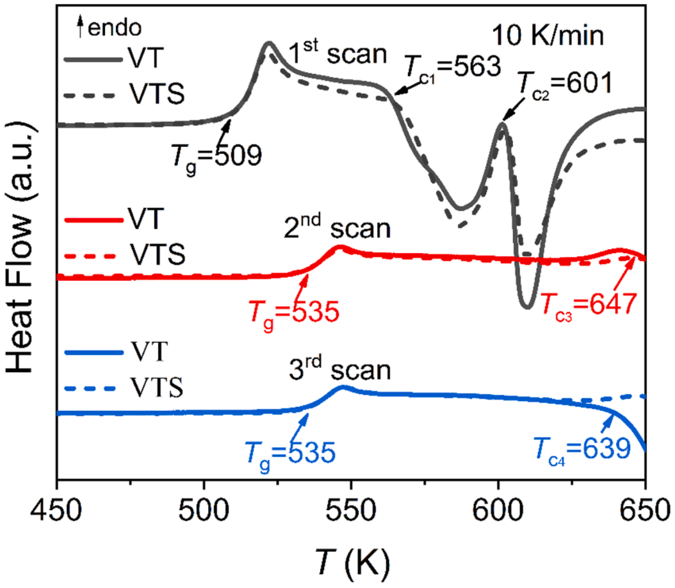

Fig. 4. DSC upscan curves of both VT (the solid line) and VTS (the dotted line), which are obtained at 10 K/min in argon. The characteristic temperatures such as T_g, T_{c1}, T_{c2}, T_{c3}, and $T_{c4}$for VT and VTS are denoted.

bonded together during heating process, NMR analysis was performed on the VTS after upscanning to different temperatures in DSC to probe their local structural changes. Fig. 1a shows the ^{29}Si spectra of VTS after upscanning to 1.1, 1.2, 1.3, 1.4, 1.6, 1.8, 2 and 2.1T_g, respectively, by DSC in argon. Each spectrum can be deconvoluted into three peaks, i.e., at ∼ −80 ppm, −85 ppm, and −110 ppm. These three peaks are attributed to crystalline Si (C-Si), amorphous Si (A-Si), and Q^4 in amorphous SiO_2 [6], respectively, where Q represents tetrahedron, and 4 is the number of bridging oxygen [7]. It can be seen that the peak at ∼ −80 ppm becomes broader and weaker with an increase of the maximum upscanning temperature (T_{max}). The peak at ∼ −85 ppm decreases and disappears at 1.6T_g while the peak at ∼ −110 ppm increases gradually. This implies that the nano-Si (both C-Si and A-Si) transformed into amorphous SiO_2 during the heating process. Fig. 1b shows the ^{51}V spectrum of VTS after scanning to different temperatures. The spectrum of each sample is deconvoluted into two components, i.e., purple and green curves, which are ascribed to [VO_4] and [VO_5], respectively, where 4 or 5 are the numbers of oxygen coordinated to each vanadium (in Fig. 1c). For VTS, as T_{max} increases, the fraction of [VO_5] increases, while that of [VO_4] decreases.

To further explore the reaction between Si and VT glass, FTIR spectra for Si, VTS-T_g, 1.1T_g, 1.2T_g were obtained and normalized by the strongest peak, as shown in Fig. 2. For the Si spectrum (black dash line), the peaks at 478cm^{-1} and at around 1000∼1250 cm^{-1} correspond to Si−O vibrations [8,9]. For the spectra of VTS-T_g, -1.1T_g, and -1.2T_g samples, peaks at 680 cm^{-1} are assigned to O−Te−O or Te−O−Te vibrations [10]. The peaks at around 985cm^{-1} are due to the vibrations of [VO_5] while the peak at 1018 cm^{-1} arises from V=O vibrations in [VO_5] [10–14]. In addition, the broad peaks locating between 750 and 940 cm^{-1} are mainly assigned to V−O−V, [VO_4], and [VO_5] vibrations and the peaks at around 1050∼1250 cm^{-1} arise from Si−O vibrations [9,10,12,15]. It should be noted that a new peak at 530 cm^{-1} is associated with the V−O−V vibration in each spectrum of VTS-1.1T_g and -1.2T_g samples, respectively [16–19]. Obviously, the intensities of peaks at 530 cm^{-1}, 985 cm^{-1}, 1018 cm^{-1}, and 1050∼1250 cm^{-1} increase with increasing T_{max}, indicating an increase in the numbers of V−O−V bonds, [VO_5] units and the Si−O bonds. This is consistent with the NMR results (Fig. 1).

Based on the NMR results in Fig. 1, the fractions of Si, SiO_2, VO_4, and VO_5 are determined by their respective deconvoluted peak areas obtained by integrating the signal intensity over the chemical shift. The fractions of both the decreased Si (i.e., $Si_{(dec.)}/(Si+SiO_2)$) and the [VO_4] transformed into [VO_5] (i.e., $VO_{4(trans.)}/(VO_4+VO_5)$), are used to assess the critical temperature, at which Si starts to react with VT glass. Specifically, $Si_{(dec.)}$ refers to the fraction of Si, which has been oxidized to Si^{4+} during heating. It is obtained by subtracting the fraction of Si in VTS heated to a temperature above T_g from that in VTS heated to T_g. $VO_{4(trans.)}$ refers to the fraction of VO_4 units that have been transformed into VO_5 during heating, which is determined by subtracting VO_4 fraction in VTS heated to a temperature above T_g from that in VTS heated to T_g. The dependences of both $Si_{(dec.)}/(Si+SiO_2)$ and $VO_{4(trans.)}/((VO_4+VO_5)$ on the T_{max}s are shown in Fig. 3. Obviously, $Si_{(dec.)}$ rises with increasing the T_{max}, interestingly, it increases drastically when T_{max} is higher than 1.4T_g, suggesting that a violent reaction occurs between Si and VT glass. In contrast, $VO_{4(trans.)}$ increases dramatically from 1.1T_g to 1.4T_g. The changes in both $Si_{(dec.)}$ and $VO_{4(trans.)}$ imply that nano-Si starts to react with VT glass at 1.1T_g. This means that the nano Si-to-SiO_2 conversion in VT glass can be controlled by varying the heat-treatment temperature.

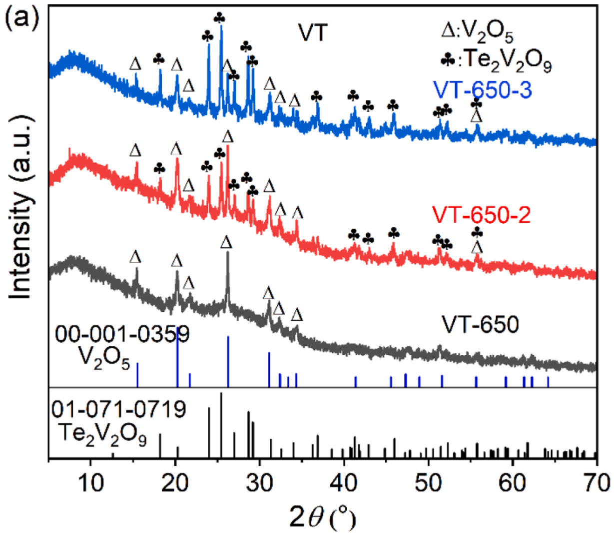

Fig. 5. XRD patterns of (a) VT and (b) VTS after the first, second and third DSC upscans to 650 K at 10 K/min in argon.

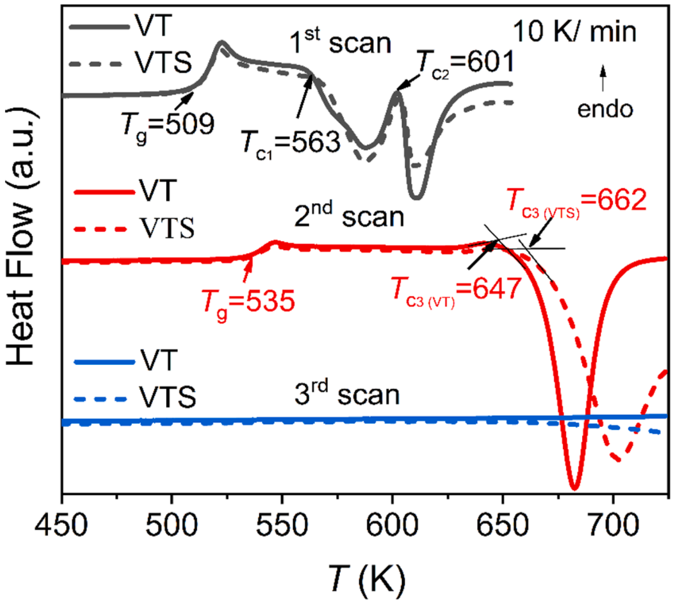

Fig. 6. DSC upscan curves of both VT (the solid line) and VTS (the dotted line), which are obtained at 10 K/min in argon. The 1st DSC upscan was performed to 650 K, and the 2nd and 3rd upscans were performed to 725 K. The characteristic temperatures such as T_g, T_{c1}, T_{c2}, and T_{c3} for VT and VTS are denoted.

Since Si can react with VT glass during the heating process, it is important to find out whether the Si-doping affects the crystallization behavior of VT glass. Fig. 4 shows the DSC upscan curves of the VT and the VTS to 650 K for three times at 10 K/min, and according to the number of the upscans, the samples are denominated as VT-650, VTS-650, VT-650-2, VTS-650-2, VT-650-3, and VTS-650-3, respectively. The T_g of both VT and VTS shifts to a higher temperature from the first to the 2nd upscan due to the crystallization in the first upscan. Then T_gs remain constant in the subsequent upscans. In addition, the T_g of VT is the same as that of VTS at each upscan, implying that the remaining glass phase in VT and VTS after crystallization might have the same composition. The two exothermic peaks with onset temperatures of T_{c1} and T_{c2} (see the first DSC upscans), respectively, do not appear in the 2nd and 3rd DSC upscan curves. However, new crystallization peaks with onset temperatures of T_{c3} and T_{c4} occur for VT but not for VTS, suggesting that the crystallization in VT glass was suppressed by introducing nano-Si.

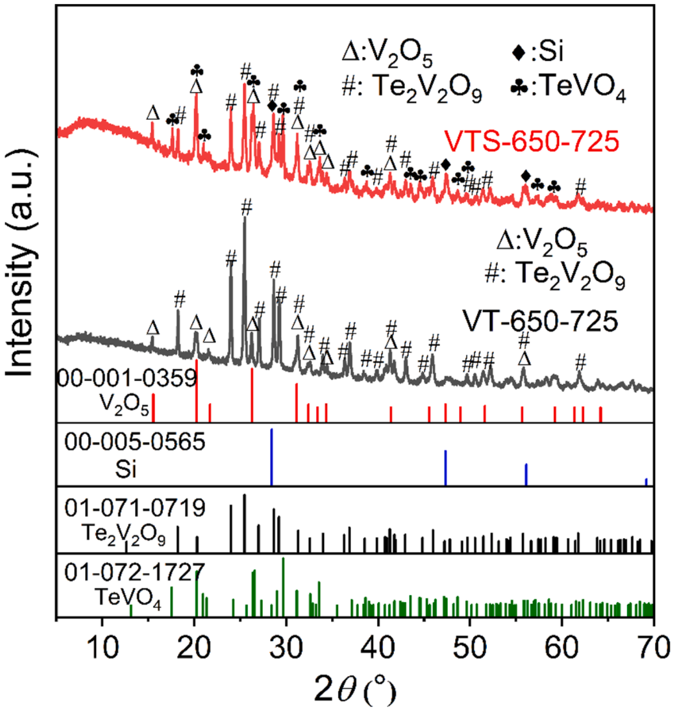

Fig. 7. XRD patterns of VT and VTS after two DSC upscans at 10 K/min in argon. The first upscan was performed to 650 K and then the second one was to 725 K, which are referred to as VT-650-725 and VTS-650-725, respectively.

Fig. 5 shows the XRD patterns of VT and VTS after the first, second and third DSC upscans to 650 K. The VT-650 sample shares the same XRD pattern as that of VTS-650, from which the V_2O_5 crystals can be identified. The precipitation of V_2O_5 increases the connectivity of the structural network according to a previous study [20], and thereby increasing T_g. However, $Te_2V_2O_9$ crystals are found in VT-650-2 and VT-650-3, but not in the corresponding VTS samples. This implies that the crystallization of $Te_2V_2O_9$ has been suppressed by introducing nano-Si into VT glass. In addition, this finding suggests that although the VT and VTS samples have the same T_g for both the 2nd and 3rd upscan curves, the compositions of the remaining glass matrices are different between the two samples.

To further explore the effect of nano-Si on the crystallization of VT

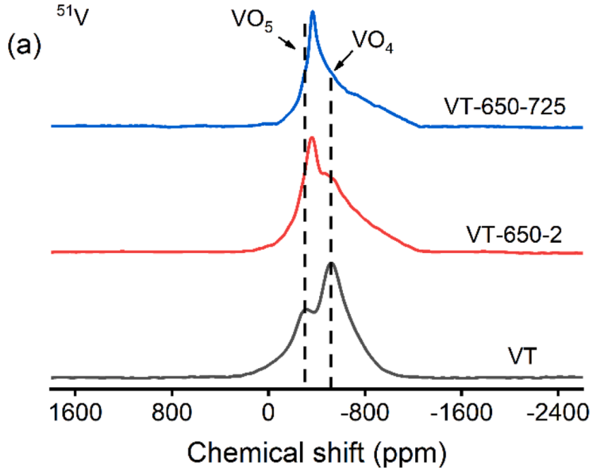

Fig. 8. ^{51}V NMR spectra of (a) VT and (b) VTS samples before and after two different DSC upscan protocols at 10 K/min in argon. One is to upscan VT and VTS to 650 K twice (VT-650-2, VTS-650-2), the other is to upscan VT and VTS to 650 K first and then to 725 K (VT-650-725, VTS-650-725).

Table 2
The fraction of VO_5 and VO_4, which were obtained from the deconvoluted ^{51}V NMR spectra shown in Fig. S2.

Sample Name	VO_5 (%)	VO_4 (%)	VO_5/VO_4	Sample Name	VO_5 (%)	VO_4 (%)	VO_5/VO_4
VT	62.2	37.8	1.65	VTS	62.3	37.7	1.65
VT-650-2	80.9	19.1	4.24	VTS-650-2	75.8	24.2	3.13
VT-650-725	88.1	11.9	7.40	VTS-650-725	88.2	11.8	7.47

glass, VT and VTS were upscanned to 650 K firstly and then to 725 K for the 2nd and 3rd times as shown in Fig. 6. Like the results in Fig. 4, the T_gs of both VT and VTS increase from the first to the second DSC upscan. However, the T_{c3} (662 K) of VTS-650-725 sample is higher than that (647 K) of VT-650-725, further confirming that the crystallization corresponding to T_{c3} is suppressed by introducing nano-Si into VT glass. In addition, the glass transitions do not occur in both VT-650-725-2 and VTS-650-725-2, implying that the glasses are fully transformed into crystal phase during the second DSC upscan.

Fig. 7 shows the XRD patterns of VT-650-725 and VTS-650-725, respectively. The Bragg peaks in the XRD pattern of VT-650-725 are attributed to V_2O_5 and $Te_2V_2O_9$. Besides these two crystalline phases, another crystalline phase, i.e., $TeVO_4$ is identified in the VTS-650-725. In other words, although the crystallization of $Te_2V_2O_9$ in VT glass is suppressed to some extent by introducing nano-Si, a new crystalline phase ($TeVO_4$) is precipitated during this process. The formation of $TeVO_4$ could be caused by the reaction of VT glass and nano-Si.

To probe the microstructural evolution in VT and VTS samples after different DSC scans, ^{51}V and ^{125}Te NMR measurements were performed. The deconvolutions of ^{51}V and ^{125}Te spectra were conducted based on chemical shift anisotropy (CSA) model [21]. Fig. 8 shows the ^{51}V NMR spectra of VT, VTS, VT-650-2, VTS-650-2, VT-650-725, and VTS-650-725, respectively. The spectrum of each sample is deconvoluted into two components (purple and green curves), which are ascribed to VO_4 and VO_5, respectively (Fig. S2). The fractions of VO_4 and VO_5 in each sample are shown in Table 2. As T_{max} increases, the VO_5/VO_4 ratio increases for both VT and VTS. Moreover, the VO_5/VO_4 ratio is higher in VT-650-2 than that in VTS-650-2. This is due to the fact that both $Te_2V_2O_9$ and V_2O_5 crystals, in which the majority of vanadium exist in VO_5 [22–28], are precipitated in VT-650-2, while only V_2O_5 forms in VTS-650-2. The lower VO_5/VO_4 ratio in VTS-650-2 further confirms the inhibiting effects of Si on the crystallization of VT glass when the sample was heat-treated to 650 K ($\approx 1.3T_g$). When T_{max} reaches 725 K ($\approx 1.4T_g$), the VO_5/VO_4 ratio in VTS-650-725 is almost the same as that in VT-650-725. This is because the two glass samples are fully transformed into crystalline phase, as verified in Fig. 6. Although a new $TeVO_4$ phase is precipitated in VTS-650-725 besides V_2O_5 and $Te_2V_2O_9$, the majority of vanadium in $TeVO_4$ exists in VO_5 [24–27].

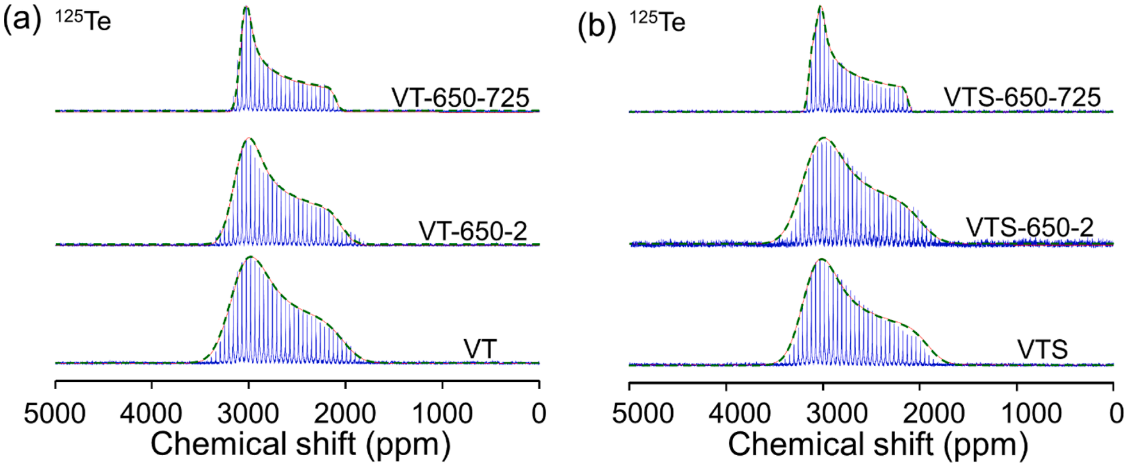

Fig. 9. ^{125}Te NMR spectra of (a) VT and (b) VTS samples before and after two different DSC upscan protocols at 10 K/min in argon. One is to upscan VT and VTS to 650 K twice (VT-650-2, VTS-650-2), the other is to upscan VT and VTS to 650 K first and then to 725 K (VT-650-725, VTS-650-725). Dashed lines: the fitting curves.

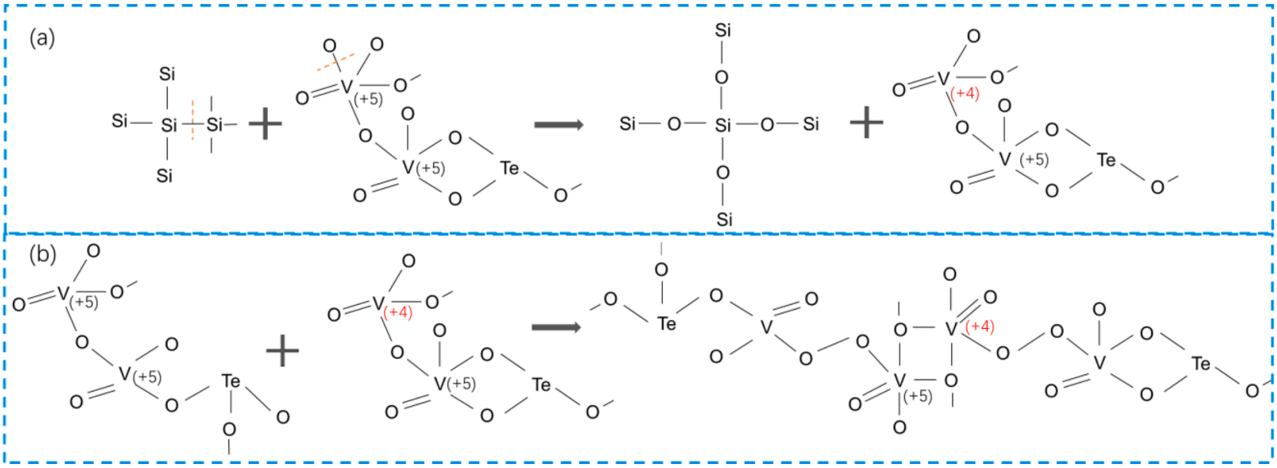

Fig. 10. Schematic diagram of the reaction between Si and VT glass (a), and the evolution of [VO_4] to [VO_5] (b) when VTS was upscanned by DSC above its T_g at 10 K/min in argon.

Fig. 9 shows the ^{125}Te NMR spectra of VT, VTS, VT-650-2, VTS-650-2, VT-650-725, and VTS-650-725. Each ^{125}Te spectrum can be represented by one unsymmetric peak, which should be ascribed to 3-coordinated Te, considering the chemical shift anisotropy (CSA) values (approximately 640-820) and the asymmetry parameters (η_{CS}) (0.1-0.2) (see Table S1) [29,30]. The peak shape of ^{125}Te spectrum becomes sharper as T_{max} rises, suggesting the transformation of glass into Te-containing crystals [23]. The sharper peak in VT-650-2 compared to that in VTS-650-2 also indicates that crystallization of $Te_2V_2O_9$ has been suppressed in VTS.

4. Discussion

As shown above, an increase of T_{max} leads to a pronounced increase both in the $Si_{(dec.)}$/(Si+SiO_2), $VO_{4(trans)}$/(VO_4+VO_5) ratios and in the number of V−O−V bonds and this indicates that the doped Si does react with VT glass. It should be mentioned that two exothermic peaks (with onset temperatures, T_{c1} and T_{c2}, respectively) consecutively occur in the 1st DSC upscan curve of VTS when heating to 650 K (Fig. 4), but only one crystalline phase (V_2O_5) is identified from the XRD pattern (Fig. 5). This could be explained by the possible scenario where the first and the second peak could be caused by the surface crystallization and the bulk crystallization (i.e., V_2O_5 formation), respectively. In addition, as shown in Fig. 6, a new crystallization peak with the onset temperature (T_{c3}) of 662 K for VTS appears, which is much larger than that for VT. This can be ascribed to the precipitation of two crystal phases $Te_2V_2O_9$ and $TeVO_4$, while only $Te_2V_2O_9$ precipitated in VT sample, as evidenced by the XRD patterns in Fig. 7. This means that two phases (V_2O_5 and $Te_2V_2O_9$) exist in VT-650-725, whereas, besides Si, three phases (V_2O_5, $Te_2V_2O_9$, and $TeVO_4$) occur in VTS-650-725 (Fig. 7).

Based on the NMR results in Fig. 1, the reaction of Si with oxygen leads to formation of amorphous SiO_2, where Si is tetrahedrally bonded to 4 bridging oxygen, during heating the VTS sample. One possible reaction mechanism is that Si bonds to 4 oxygens and each oxygen is provided by one [VO_5] unit in VT glass, consequently, the tetrahedral [SiO_4] network locally forms and [VO_4] units appear. Meanwhile, Si reduces V^{5+} to V^{4+}. Then, the remaining [VO_x] units rearrange themselves to the ordered structure, i.e., crystals form during the heating process to a temperature of 662 K, and simultaneously part of [VO_4] units are transformed into [VO_5] units by sharing oxygen with other [VO_4] units. Thus. the chain-like [VO_4] structure are converted into zigzag [VO_5] structure (Fig. 10) [23], generating new V−O−V bonds as verified by NMR and FTIR results shown in Fig. 2.

In addition, introducing nano-Si into VT glass has only a minor effect on formation of V_2O_5, but can suppress the crystallization of $Te_2V_2O_9$ during the first and second DSC upscans to 650 K. When the T_{max} is increased to 725 K, both $Te_2V_2O_9$ and $TeVO_4$ crystals formed for VTS (Fig. 7). However, the onset temperature (T_{c3}) of the crystallization peak for VTS glass is higher than that of VT glass (see Fig. 6). This means that the nano-Si has the suppressing effect on crystallization of VT glass. To uncover the crystallization-suppressing mechanism of Si on VT glass, it is important to clarify the redox reaction between Si and VT glass. In this regard, we need to derive the redox reaction equation for *n* moles of VT glass. During the first upscan to 650 K, since only a small amount of Si particles has reacted with VT glass, the moles of the original glass can be approximately considered to be *n* moles. After the first upscan to 650 K, *k* moles V_2O_5 crystals are assumed to precipitate from the glass matrix. Thus, the chemical formula of the remaining glass (R-glass) is expressed as $Te_nV_{2(n\text{-}k)}O_{7n\text{-}5k}$ ($n>k$, $n>0$, $k>0$). Assuming that the molar amounts of the reacted Si and R-glass are *x* and *y*, respectively, during the second DSC scan, then the reaction can be written as:

$$xSi + yTe_nV_{2(n-k)}O_{7n-5k} \rightarrow yTe_nV_{2(n-k)}O_{7n-5k-2x} + xSiO_2(amorphous) \tag{1}$$

Among the four types of elements in the VTS sample, only vanadium is polyvalent, since it can exist as V^{5+} and V^{4+}. Therefore, considering the charge balance of the reaction, Si reduces V^{5+} to V^{4+}. Thus, we get the equations:$4x = 2y(n-k)$, then $x = \frac{y(n-k)}{2}$. In addition, owing to the conservation of oxygen ions, the relation $y(7n-5k) = y(7n-5k-2x) + 2x$ should be valid, from which y is found to be 1. Since the new crystal ($TeVO_4$) is precipitated from VTS-650-725, the values of *n* and *k* can be 2 and 1, respectively. Hence, reaction (1) can be rewritten as:

$$\frac{1}{2}Si + Te_2V_2O_9(glass) \rightarrow Te_2V_2O_8(2TeVO_4)(glass) + \frac{1}{2}SiO_2(amorphous) \tag{2}$$

During the first and second DSC upscan to 650 K, in addition to the energy used to overcome the energy barrier for V_2O_5 formation, the remaining energy is preferentially consumed for the reaction (2). However, when increasing T_{max} of the second upscan to 725 K, the thermal energy is sufficient for overcoming the energy barrier for both the precipitation of $Te_2V_2O_9$ and $TeVO_4$ crystals and that for reaction (2).

5. Conclusions

We prepared a composite material that is composed of nano-Si and V_2O_5-TeO_2 glass (VT) to be potentially applied as the anode material for advanced LIBs. The nano-Si is physically mixed with the VT glass, and then the mixture was subjected to different dynamic heat-treatment in argon. By using both solid-state NMR and FTIR techniques, we clarified both the reaction mechanism of nano-Si with VT glass and their crystallization behavior. The nano-Si reacted with VT glass at $\geq 1.1T_g$ (560 K), leading to formation of amorphous SiO_2. The nano Si-to-SiO_2 conversion in VTS glass can be controlled by designing the heating protocol.

Moreover, it was found that introducing nano Si into VT glass could suppress the formation of $Te_2V_2O_9$ crystals during heating to 650 K ($1.3T_g$) but induce the formation of $TeVO_4$ during heating to a higher temperature 725 K ($1.4T_g$). This was explained by the redox reaction between nano-Si and the remaining glass after V_2O_5 precipitation. That is, during the heating of VTS sample, V_2O_5 was precipitated. After that, nano-Si reacted with $Te_2V_2O_9$ glass phase, leading to formation of amorphous SiO_2 and $TeVO_4$ glass phase. Differing from the crystallization in VT glass under the same heating condition, the crystallization in VTS glass requires more thermal energy to overcome the energy barrier for redox reaction (2), thereby making the formation of $Te_2V_2O_9$ crystals more difficult. When VTS was heated to a higher temperature 725 K ($1.4T_g$), the energy is sufficient for formation of both $TeVO_4$ and $Te_2V_2O_9$ phases. This work helps design Si-oxide glass composites for a specific application, e.g., in high performance LIBs.

CRediT authorship contribution statement

Jiajia Yan: Investigation, Methodology, Data curation, Writing – original draft. **Tongyao Zhao:** Investigation, Data curation. **Nian Shi:** Investigation, Data curation. **Hongbing Zhan:** Writing – review & editing. **Jinjun Ren:** Methodology, Data curation, Writing – review & editing. **Yanfei Zhang:** Conceptualization, Methodology, Writing – review & editing. **Yuanzheng Yue:** Supervision, Methodology, Conceptualization, Writing – review & editing.

Declaration of Competing Interest

The authors declare that they have no known competing financial interests or personal relationships that could have appeared to influence the work reported in this paper.

Acknowledgments

Authors would like to acknowledge support by National Natural Science Foundation of China (Nos. U1732155, 51672045, 51772223), China Scholarship Council (201906650022), Taishan Youth Scholar Project of Shandong Province (tsqn202103098), and Shandong Provincial Natural Science Foundation (ZR2020ME025).

Supplementary materials

Supplementary material associated with this article can be found, in the online version, at doi:10.1016/j.jnoncrysol.2022.121651.

References

[1] D.H. Tan, Y.T. Chen, H. Yang, W. Bao, B. Sreenarayanan, J.M. Doux, W. Li, B. Lu, S. Y. Ham, B. Sayahpour, Carbon-free high-loading silicon anodes enabled by sulfide solid electrolytes, Science 373 (2021) 1494–1499.
[2] Y.F. Zhang, P. Wang, T. Zheng, D. Li, G. Li, Y. Yue, Enhancing Li-ion battery anode performances via disorder/order engineering, Nano Energy 49 (2018) 596–602.
[3] Y.F. Zhang, P.X. Wang, G.D. Li, J.H. Fan, C.W. Gao, Z.Y. Wang, Y.Z. Yue, Clarifying the charging induced nucleation in glass anode of Li-ion batteries and its enhanced performances, Nano Energy 57 (2019) 592–599.
[4] J. Kjeldsen, Y. Yue, C.B. Bragatto, A.C. Rodrigues, Electronic conductivity of vanadium-tellurite glass-ceramics, J. Non Cryst. Solids 378 (2013) 196–200.
[5] X. Liu, Heterogeneous nucleation or homogeneous nucleation? J. Chem. Phys. 112 (2000) 9949–9955.
[6] P. Pena, J.R. Mercury, A. De Aza, X. Turrillas, I. Sobrados, J. Sanz, Solid-state ^{27}Al and ^{29}Si NMR characterization of hydrates formed in calcium aluminate–silica fume mixtures, J. Solid State Chem. 181 (2008) 1744–1752.
[7] J. Xu, X. Wang, H. Fu, C.M. Brown, X. Jing, F. Liao, F. Lu, X. Li, X. Kuang, M. Wu, Solid-state ^{29}Si NMR and Neutron-diffraction studies of $Sr_{0.7}K_{0.3}SiO_{2.85}$ oxide ion conductors, Inorg. Chem. 53 (2014) 6962–6968.
[8] I. Joni, L. Nulhakim, M. Vanitha, C. Panatarani, Characteristics of crystalline silica (SiO_2) particles prepared by simple solution method using sodium silicate (Na_2SiO_3) precursor, J. Phys. Conf. Ser. 1080 (2018), 012006.
[9] W. Yang, W. Huang, Q. Zheng, W. Huang, Z. Chen, High efficiency preparation, structure and properties of silicon nano-crystals by induction plasma method, NanoWorld J. 2 (2016) 63–68.
[10] S. Rada, E. Culea, V. Rus, M. Pica, M. Culea, The local structure of gadolinium vanado-tellurite glasses, J. Mater. Sci. 43 (2008) 3713–3716.
[11] A. Rahim, A. Arof, Spectroscopic studies of V_2O_5–Bi_2O_3–TeO_2 glasses, Opt. Quantum Electron. 48 (2016) 238.
[12] Y. Saddeek, I. Yahia, W. Dobrowolski, L. Kilanski, N. Romcevic, M. Arciszewska, Infrared, Raman spectroscopy and ac magnetic susceptibility of Gd_2O_3-TeO_2-V_2O_5 glasses, Optoelectron. Adv. Mater. Rapid Commun. 3 (2009) 559–564.
[13] V. Murgia, E.M.F. Torres, J.C. Gottifredi, E.L. Sham, Sol gel synthesis of V_2O_5–SiO_2 catalyst in the oxidative dehydrogenation of n-butane, Appl. Catal. A Gen. 312 (2006) 134–143.
[14] T. Srikumar, C.S. Rao, Y. Gandhi, N. Venkatramaiah, V. Ravikumar, N. Veeraiah, Microstructural, dielectric and spectroscopic properties of Li_2O–Nb_2O_5–ZrO_2–SiO_2 glass system crystallized with V_2O_5, J. Phys. Chem. Solids 72 (2011) 190–200.
[15] K. Shafeeq, V. Athira, C.R. Kishor, P. Aneesh, Structural and optical properties of V_2O_5 nanostructures grown by thermal decomposition technique, Appl. Phys. A 126 (2020) 1–6.
[16] W. Chen, J. Peng, L. Mai, H. Yu, Y. Qi, Synthesis and characterization of novel vanadium dioxide nanorods, Solid State Commun. 132 (2004) 513–516.
[17] M.M. Islam, M.A. Rashid, M.P. Ahamed, M.E. Hossain, M.R. Ahsan, M.G. Mortuza, M.H.K. Rubel, Morphogenesis of silicovanadate glasses: investigation of physical properties, J. Eng. Adv. (2021) 78–86.
[18] H. Ji, D. Liu, H. Cheng, C. Zhang, L. Yang, D. Ren, Infrared thermochromic properties of monoclinic VO_2 nanopowders using a malic acid-assisted hydrothermal method for adaptive camouflage, RSC Adv. 7 (2017) 5189–5194.
[19] X. Wu, Z. Wu, C. Ji, H. Feng, X. Ma, Y. Su, Y. Zhou, J. Wang, Y. Jiang, Influence of infrared optical properties by transformation of the crystal structure in Al-doped vanadium dioxide films, Opt. Mater. Express 6 (2016) 3500–3506.
[20] S. Chakraborty, P. Boolchand, M. Malki, M. Micoulaut, Designing heavy metal oxide glasses with threshold properties from network rigidity, J. Chem. Phys. 140 (2014), 014503.
[21] M. Bak, J.T. Rasmussen, N.C. Nielsen, SIMPSON: a general simulation program for solid-state NMR spectroscopy, J. Magn. Reson. 213 (2011) 366–400.
[22] C.J. Fontenot, J.W. Wiench, G.L. Schrader, M. Pruski, ^{17}O MAS and 3QMAS NMR investigation of crystalline V_2O_5 and layered $V_2O_5 \cdot nH_2O$ Gels, J. Am. Chem. Soc. 124 (2002) 8435–8444.
[23] S. Sakida, S. Hayakawa, T. Yoko, ^{125}Te and ^{51}V static NMR study of V_2O_5-TeO_2 glasses, J. Phys. Condens. Matter. 12 (2000) 2579.
[24] M.I. Aroyo, A. Kirov, C. Capillas, J. Perez-Mato, H. Wondratschek, Bilbao Crystallographic Server. II. Representations of crystallographic point groups and space groups, Acta Crystallogr. Sect. A Found. Crystallogr. 62 (2006) 115–128.
[25] M.I. Aroyo, J.M. Perez-Mato, C. Capillas, E. Kroumova, S. Ivantchev, G. Madariaga, A. Kirov, H. Wondratschek, Bilbao crystallographic server: I. Databases and crystallographic computing programs, Z. Kristallogr. 221 (2006) 15–27.
[26] M. Vergniory, L. Elcoro, C. Felser, N. Regnault, B.A. Bernevig, Z. Wang, A complete catalogue of high-quality topological materials, Nature 566 (2019) 480–485.
[27] M.I. Aroyo, J. Perez-Mato, D. Orobengoa, E. Tasci, G. de la Flor, A. Kirov, Crystallography online: bilbao crystallographic server, Bulg. Chem. Commun. 43 (2011) 183–197.
[28] B. Bradlyn, L. Elcoro, J. Cano, M. Vergniory, Z. Wang, C. Felser, M. Aroyo, B. A. Bernevig, Topological quantum chemistry, Nature 547 (2017) 298–305.
[29] S. Sakida, S. Hayakawa, T. Yoko, Part 2 ^{125}Te NMR study of M_2O–TeO_2 (M= Li, Na, K, Rb and Cs) glasses, J. Non Cryst. Solids 243 (1999) 13–25.
[30] Z. Jiang, T. Zhao, J. Ren, Y. Zhang, Y. Yue, NMR evidence for the charge-discharge induced structural evolution in a Li-ion battery glass anode and its impact on the electrochemical performances, Nano Energy 80 (2021), 105589.